https://doi.org/10.5194/egusphere-2025-1325
Preprint. Discussion started: 1 April 2025

Passive seismic imaging of the Lower Palaeozoic in the Sudret area of Gotland, Sweden

Zhihui Wang[1,2], Christopher Juhlin[2,*], Peter Hedin[3], Mikael Erlström[4], Daniel Sopher[3]

[1]Chinese Academy of Geological Sciences, Beijing, 100037, China
[2]Uppsala University, Department of Earth Sciences, Uppsala, 75236, Sweden
[3]Geological Survey of Sweden, Uppsala Office, Uppsala, 75128, Sweden
[4]Lund University, Department of Geology, Lund, 22362, Sweden

Correspondence to: Christopher Juhlin (christopher.juhlin@geo.uu.se)

Abstract. Passive seismic data were acquired together with active seismic data along a 2.8 km long profile in the Sudret area of Gotland, Sweden, as part of a feasibility study for storage of CO_2 below the Baltic Sea. Seismic interferometry using cross-correlation and cross-coherence was employed on the passive seismic data. Correlation was used to retrieve virtual shot gathers containing mainly surface waves, while cross-coherence was used to retrieve mainly seismic reflections. Inversion for shear wave velocity and CDP processing of the passive data result in velocity profiles and images that correlate well with borehole data, synthetic seismograms and the active seismic data. Both the passive surface wave and body wave results provide geological information which complement the active data, the surface waves providing S-wave velocity information and the body waves providing a lower frequency image. The passive data are consistent with the active data and there is no indication of any large-scale faults in the area. Furthermore, analysis of the frequency and direction of the ambient noise using power spectral density and beam forming shows that ocean waves and human activity around the island of Gotland makes the Sudret area an ideal location for passive imaging. Our results illustrate that passive seismic imaging can be an important complement to active seismic data for evaluating the subsurface with respect to CO_2 storage and monitoring in the Gotland area, Sweden, and perhaps, elsewhere.

Keywords

Passive seismic; Carbon capture and storage; Ambient noise; Seismic interferometry; Virtual shot gathers

1 Introduction

Carbon capture and storage (CCS) is a strategy that can be employed for reducing atmospheric emissions of greenhouse gases and thereby their adverse effects on the climate (Niemi et al., 2017). A large theoretical capacity to store carbon dioxide (CO_2) in the Palaeozoic sedimentary successions within the Baltic Basin exists, including large saline aquifers and depleted oil and gas fields (Anthonsen, 2013; Sopher et al., 2014; Shogenova et al., 2021). Identification and characterization of potential storage sites are important cornerstones for establishing safe geological storage of CO_2 (Lüth et al., 2017). In Sweden, sedimentary strata potentially suitable for CO_2 storage are only found in the Baltic Basin, south of Gotland and in

https://doi.org/10.5194/egusphere-2025-1325
Preprint. Discussion started: 1 April 2025

southwest Skåne and adjacent offshore areas. During the past few years, the Geological Survey of Sweden (SGU) has been investigating suitable locations for CO_2 storage offshore. Two Swedish marine areas with potential for storage are being investigated, one south of Skåne in southern Sweden and one in the southeastern Baltic (www.sgu.se). These areas contain deeply seated porous reservoir sandstones capped by thick caprock which could provide the prerequisites for safe storage of CO_2. Because drilling at sea is costly, as well as complex, two boreholes were drilled down to about 800 m in the Sudret area on south Gotland where the sandstones are found deepest onshore and can be used as analogs to the offshore area. In November, 2023 reflection seismic data were acquired in the vicinity of the two boreholes to provide a better understanding of the sedimentary strata and the local subsurface structural framework, (Juhlin et al., 2025).

Active seismic reflection surveying and distributed acoustic sensing (DAS) with high resolution have been the dominant methods for imaging and monitoring CO_2 storage sites (Juhlin et al., 2007; Alcalde et al., 2014; Pevzner et al., 2015; Roach et al., 2015; White et al., 2015, 2022; Huang et al., 2016; Zhang et al., 2016; Cheraghi et al., 2017; Harris et al., 2017; Lüth et al., 2017; Ivandic et al., 2018; Papadopoulou et al., 2023, 2024; Wang and Lawton, 2024; Zappalà et al., 2024). However, active-source seismic surveys suffer from the high cost of data acquisition and lack of continuous monitoring for sudden temporal variations (Ikeda et al., 2017). Several studies show that passive seismic surveying could be a complement to CO_2 geological storage monitoring (De Ridder and Biondi, 2012; Riahi et al., 2013; Boullenger et al., 2015; Gassenmeier et al., 2015; Cheraghi et al., 2017; Cao and Askari, 2019; Xu et al, 2012; Hassing et al., 2024). Potential advantages of the technique are that it is relatively environmentally friendly and cost effective, as it uses ambient noise as a source.

Our investigation recorded 14-hours of continuous passive data along a 2.8 km long profile to retrieve virtual shot gathers using seismic interferometry. Subsequently, standard surface wave and seismic reflection data processing were employed to obtain a shear wave velocity model and a seismic reflection stacked section. Both the body waves and surface waves provide high-quality images and have good consistency with the borehole section, geophysical logging and the active seismic data from the same location. Moreover, the results reveal some reliable deep geological information which the active data could not provide because of the limited source energy. Finally, we show that the frequency content and direction of the ambient noise makes the Sudret area an ideal location for passive imaging.

2 Geological setting of the test site

The test site is located on Sudret, the southernmost part of the island of Gotland, located in the central part of the Baltic Sea (Fig. 1a). The present investigation is furthermore focused around the cored borehole Nore-1 drilled in 2024 to 791 m depth (Erlström et al., 2024). Nore-1 and the neighboring Nore-2 were drilled by the Geological Survey of Sweden in 2023 within a CO_2 investigation program launched by the Swedish Government with the objective to investigate three potential Cambrian sandstone reservoirs, as well as studying the overlying Ordovician and Silurian sealing strata. The Nore-1 borehole

https://doi.org/10.5194/egusphere-2025-1325
Preprint. Discussion started: 1 April 2025

intersected a 778 m thick sedimentary succession on top of the porphyritic potassium-rich granite basement (Fig. 1b and 1c). At the base of the sedimentary succession there is a c. 220 m thick Lower and Middle Cambrian interval which includes three 20 to 50 m thick sandstone units, i.e. the Viklau, När and Faludden sandstones, with intermediate layers of silty claystone and mudstone. The three potential reservoirs for CO_2 storage are located at the depths of 554–575 m, 677–706 m and 728–778 m, respectively. The uppermost unit, i.e. the Faludden Sandstone, is the most promising candidate for CO_2 storage. The overlying Ordovician interval between 472 m and 554 m depth comprises variably argillaceous limestone and calcareous mudstone. The top of the Ordovician generates a clear reflection in the active seismic data. One interval in the Ordovician, between 492 and 505 m depth, stands out due to its bentonite and mudstone layers. This unit is consistent between wells on Gotland and can be identified in most of the available geophysical well logs. Furthermore, with relatively high frequency seismic reflection data, a reflection can be observed to be associated with this interval (Erlström and Sopher, 2019). Overlying the Ordovician is a 472 m thick Silurian succession, which from 118 m depth down to the Ordovician mainly comprises marlstone and calcareous claystone with subtle lithological variations. Besides a 55 m thick mudstone above the Ordovician, and two relatively thin limestone-dominated intervals at 400 m and 310 m, which can be correlated between wells, most of the interval between 118–472 m is poorly lithostratigraphically defined. The uppermost part of the Silurian from 118 m depth to the top of the bedrock consists of a mixed interval with limestone, mudstone, sandstone and reef limestone, representing the Eke, Burgsvik and Hamra-Sundre formations. The Eke limestone between 107 m and 118 m stands out as a significant marker in the geophysical logs in all wells on south Gotland. Above the Eke limestone follows the c. 50 m thick Burgsvik interval with alternating layers of fine-grained sandstone and calcareous mudstone. The uppermost part of the Silurian present in the Sudret area consists of relatively coarse-grained carbonates of the Hamra and Sundre formations. The Quaternary deposits are up to c. 4 m thick in the study area and mainly consist of sandy and pebbly deposits.

https://doi.org/10.5194/egusphere-2025-1325
Preprint. Discussion started: 1 April 2025

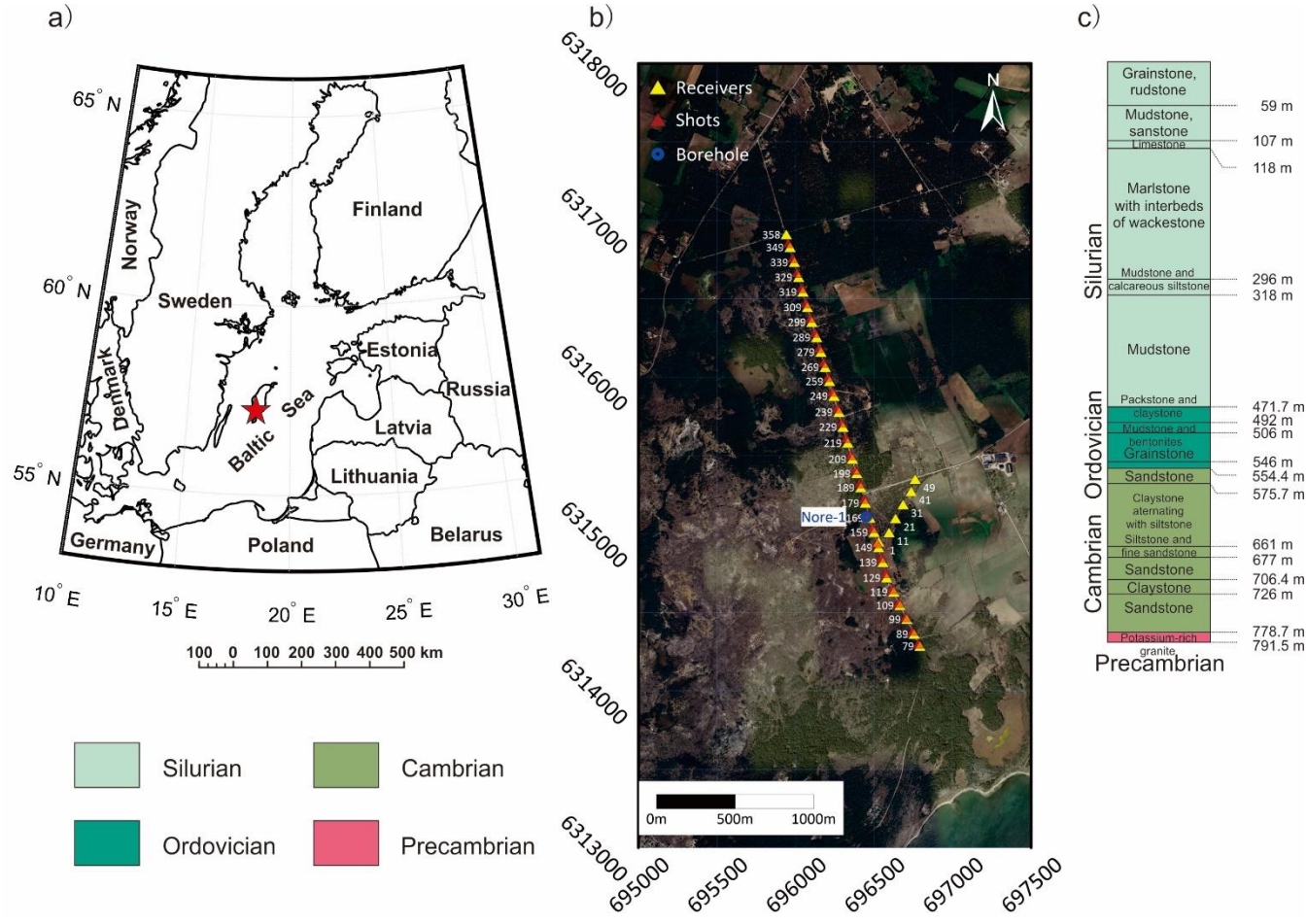

Figure 1: (a) The experimental site shown as the red star located in southern Gotland, Sweden. (b) Locations of survey line and borehole Nore-1. For clarity, every tenth receiver and source location are shown. Receivers are marked by the yellow triangles, and source locations are represented by the orange triangles. Both receiver spacing and source spacing were 10 m. The blue hollow circle shows the Nore-1 borehole location (the aerial image from © Google Maps) (c) Mapped Nore-1 borehole lithology.

3 Data acquisition and processing

3.1 Active and passive data acquisition

In order to image the subsurface down to the Precambrian basement in the vicinity of the two boreholes that had been drilled earlier and to investigate if any faults could be observed in the sedimentary strata a 2D active seismic survey was carried out from 12 November, 2023 to 13 November, 2023. This 2D survey was part of a larger investigation of the area that included a small 3D survey (Juhlin et al., 2025). A skid-steer loader with a 500 kg weight drop hammer with plate was used as a source and 329 5 Hz SmartSolo nodal units were available for recording. After acquiring the active data, 14-hours of continuous

https://doi.org/10.5194/egusphere-2025-1325
Preprint. Discussion started: 1 April 2025

passive data (Table 1) were recorded along the 2.8 km long profile with 10 m receiver spacing and 1 ms sample rate (Wang et al., 2024).

Table 1: Active and passive seismic data acquisition parameters for the Sudret area on Gotland, Sweden.

	Passive Seismic Data	Active Seismic Data
Recording system	Smart Solo	Smart Solo
Receiver	IGU-16HR 1C, 5Hz	IGU-16HR 1C, 5Hz
Source		500 kg weight drop hammer
Receiver interval	10 m	10 m
Shot interval	10 m	10 m
CMP interval	5 m	5 m
Sampling rate	1 ms	1 ms
Recording length	14 hours	2 s
Minimum offset	0 m	0 m
Maximum offset	2800 m	2800 m
Survey geometry	Asymmetric split spread, fixed-geophone locations	
Number of receivers	280	280
Number of source points	280	277

3.2 Data pre-processing

Prior to applying seismic interferometry, standard data pre-processing was applied to the ambient noise data (Table 2). We removed the mean and de-trended the recordings and afterwards separated 14 hours of continuous ambient data into 8400 segments with 6 s length. Then, normalization and bandpass filtering with different parameters were applied to separate the surface and body waves from the ambient noise data. For the surface waves, a bandpass filter with corner frequencies of 0.5-1-40-50 Hz was used and followed by normalization in the time domain. For the body waves, a bandpass filter with corner frequencies of 5-6-20-25 Hz and spectral whitening in the frequency domain were applied to suppress surface waves and enhance reflected energy.

https://doi.org/10.5194/egusphere-2025-1325
Preprint. Discussion started: 1 April 2025

110

Table 2. Passive data processing workflow and parameters.

Step	Processing workflow	
	Surface waves	**Body waves**
1	Data input, read SEGD format data	Data input, read SEGD format data
2	Data segment (6 s)	Data segment (6s)
3	De-meaning and De-trending	De-meaning and De-trending
4	Band pass filter (0.5-1-40-50 Hz)	Band pass filter (5-6-20-25 Hz)
5	Time domain normalization, one-bit	Frequency domain normalization, spectral whitening
6	Cross correlation	Cross coherence
7	Dispersion curve calculation	Geometry, CMP binning: 5m
8	Velocity inversion	Spectral Equalization, 5-6-18-19Hz
9	Data output	Median filter, airwaves 340 m/s,
10		Surgical muting, mute above first breaks
11		Velocity analysis
12		NMO, 70% stretch
13		Stack
14		F-X deconvolution, window length 19 traces
15		Band-pass filter 5-6-18-19 Hz

3.3 Retrieving Green's function by cross-correlation and cross coherence

The wavefield generated by a noise source can be represented by the convolution of the source wavelet and a Green's
115 function. Since Claerbout (1968) first proposed that the reflection response of a horizontally layered medium can be obtained from one side of the autocorrelation of its transmission response, different seismic interferometry techniques have been developed and improved to retrieve the Green's function and characterize the seismic wave propagation between two

https://doi.org/10.5194/egusphere-2025-1325
Preprint. Discussion started: 1 April 2025

receivers (Cole, 1995; Rickett and Claerbout, 1999; Schuster, 2001; Campillo and Paul, 2003; Bakulin and Calvert, 2006; Draganov et al, 2009; Wapenaar et al., 2004, Shapiro et al., 2005; Snieder, 2004; Wapenaar and Fokkema, 2006; Prieto et al., 2009; Nakata et al., 2015; Meles et al., 2015; Olivier et al., 2015; Oren and Nowack, 2017). Here, we use cross-correlation and cross-coherence of the ambient noise data recorded at different receivers to retrieve surface wave and body wave source gathers, respectively. The cross-correlation and cross-coherence methods are reviewed in the following sections.

3.3.1 Cross-correlation

The cross-correlation of the wavefield recording retrieved from ambient noise at the locations r_A and r_B can be described as

$$C(\omega) = u(r_A, \omega)u^*(r_B, \omega) \quad (1)$$

where $u(r_A, \omega)$ and $u^*(r_B, \omega)$ respectively represent the observed wavefield in the frequency domain at the locations r_A and r_B, and the asterisk denotes the complex conjugate (Wapenaar and Fokkema, 2006).

3.3.2 Cross-coherence

Similarly, the cross-coherence of the seismic wavefield H_{AB} is defined in the frequency domain as

$$H_{AB} = \frac{u(r_A,\omega)u^*(r_B,\omega)}{|u(r_A,\omega)||u(r_B,\omega)|} \quad (2)$$

where $|u(r_A, \omega)|$ and $|u(r_B, \omega)|$ denote the amplitude of the wavefield in the Fourier domain and the asterisk denotes the complex conjugate (Nakata et al., 2011).

4 Surface wave data processing

4.1 Calculating and picking of dispersion curves

A total of 90 source gathers were retrieved by cross-correlation using equation (1) from receiver number 79 to 358 (see Fig. 1b for locations). Each retrieved source gather consists of 191 nodal units with a 3 s recording length and 0-1900 m offsets. Figure 2a shows a retrieved source gather and its dispersion diagram, the surface wave dominates in the virtual source recording and a reliable frequency curve within the window 0.8-5.5 Hz can be picked (Fig. 2b). The dispersion curves from different source gathers shown in Figure 2c have a good consistency and suggest that we have obtained high signal-to-noise ratio surface wave data and that the structural variation in the horizontal direction is minor in this area.

https://doi.org/10.5194/egusphere-2025-1325
Preprint. Discussion started: 1 April 2025

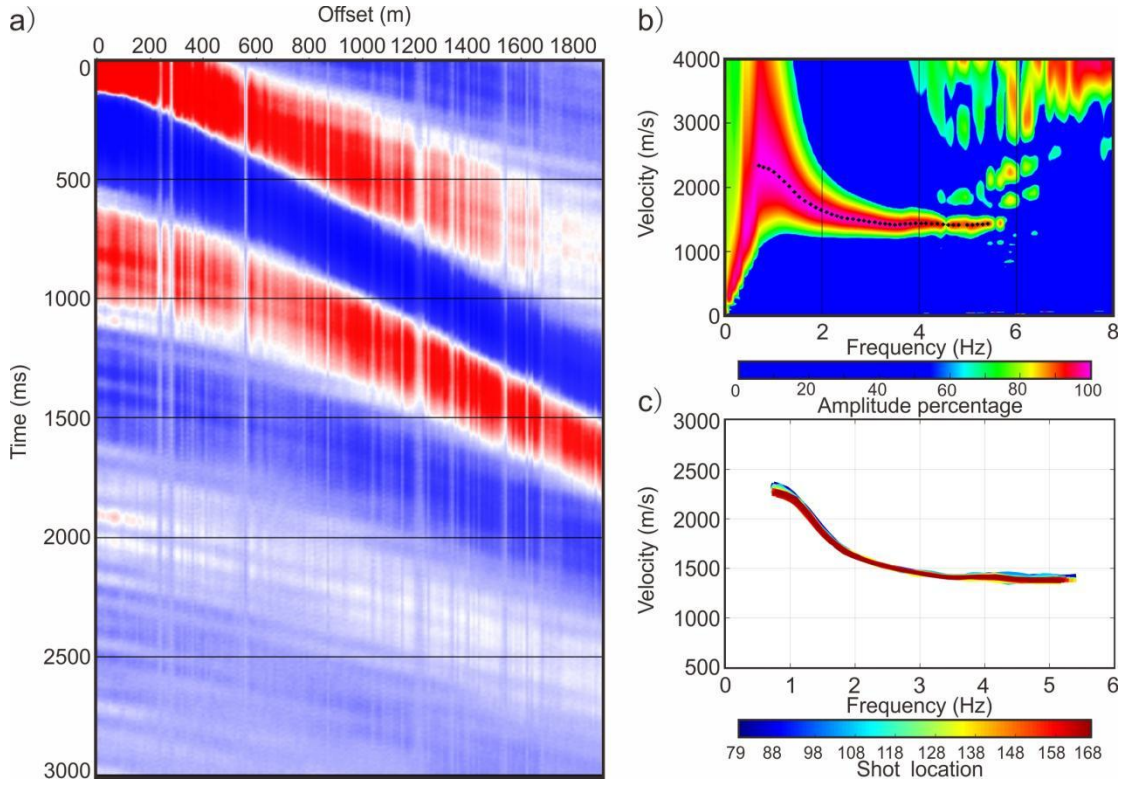

Figure 2: (a) Retrieved source gather for surface waves at source location No. 79; (b) dispersion diagram from (a); (c) Dispersion curves plot for all survey points.

4.2 Inversion for the velocity model

Rayleigh wave inversion is a nonlinear optimization problem. To avoid the solution estimate falling into a local minimum value of the objective function and to minimize the dependency on the initial model, an overall optimization based on a genetic algorithm (Zhao et al., 1995) was used to invert for the shear wave velocity model. Four different models were used as initial models to compare with the inverted results (Fig. 3a). Model 1 uses a velocity gradually increasing with depth, while model 3 was embedded with a high velocity layer at depths of 480 m to 580 m known to be present from acoustic logging data (Fig. 3b). Model 2 and model 4 were variations of model 3 and embedded with a high velocity layer between 380 m to 480 m and between 580 m to 680 m, respectively, to test the sensitivity of the inversion to the preferred starting model (model 3). A comparison of the velocity inversion results between model 1 and model 3 shows, as expected, that the inclusion of the high velocity layer in the initial model results in a better match with the acoustic log (Fig. 3b). This is also seen in the comparison between the inverted dispersion curves and the observed one (Fig. 3c and 3e). Furthermore if this high velocity layer is moved up or down in the initial model then a poorer match between the observed dispersion curve and the inverted curves is obtained (compare Fig. 3e with Fig. 3d and 3f). Accordingly, model 3 was used as the initial model to invert all dispersion curves to obtain the shear wave velocity image.

https://doi.org/10.5194/egusphere-2025-1325
Preprint. Discussion started: 1 April 2025

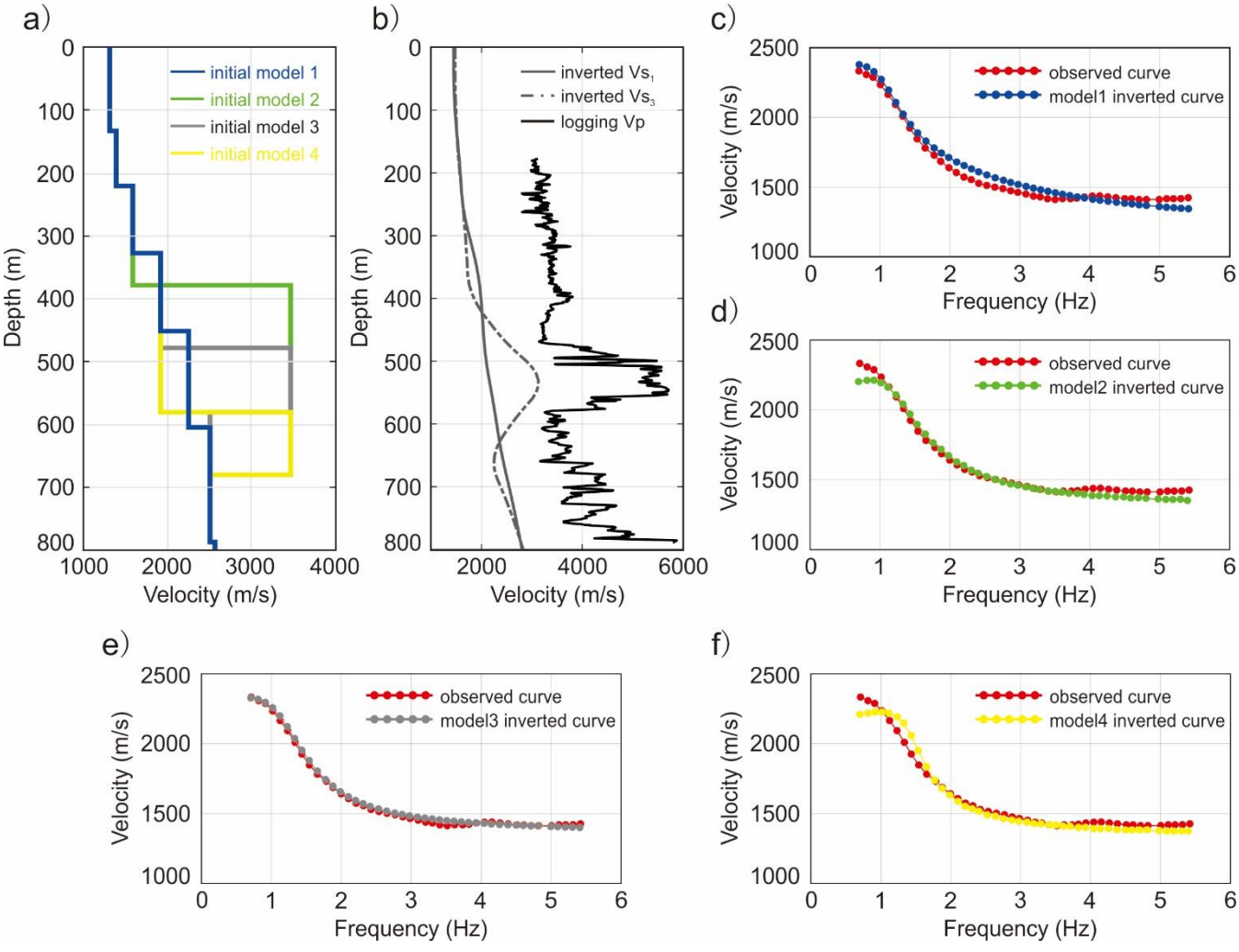

Figure 3: (a) Four different initial models for inversion, initial model 1 is a velocity gradually increasing with depth, initial model 2, initial model 3 and initial model 4 are embedded with a high velocity layer at depths of 380 m to 480 m, 480 m to 580 m and 580 m to 680 m, respectively; (b) Acoustic logging curve and inverted shear wave velocity models Vs_1 and Vs_3 are from initial model 1 and initial model 3, respectively; (c) Observed and inverted curves from initial model 1; (d) Observed and inverted curves from initial model 2 ; (e) Observed and inverted curves from initial model 3; (f) Observed and inverted curves from initial model 4.

5 Body wave data processing

A total of 290 source gathers were retrieved with fixed geometry after the cross coherence calculation. Raw source gather recordings are dominated by low frequency signals (Fig. 4d), however, a direct, or diving, P-wave with a velocity of 3700 m/s, a direct S-wave with a velocity of 1700 m/s and air waves are clear in the raw source gather (Fig. 4a). Reflections with low frequency and high amplitude are present at times of 320 ms and 500 ms. Spectral equalization in the frequency band 5-6-18-19 Hz was applied on all retrieved raw source gathers to reduce noise and enhance the weaker amplitude reflected

https://doi.org/10.5194/egusphere-2025-1325
Preprint. Discussion started: 1 April 2025

signals. Direct P-waves and reflections are present and marked with arrows in Fig. 4b. Before velocity analysis and stacking, the air waves were attenuated by a median filter at velocities of 340 m/s. Reflections are now more clearly observed in Fig. 4c. Conventional seismic reflection processing flows including surgical muting, velocity analysis, normal moveout, stacking, f-x deconvolution and bandpass filtering were carried out as outlined in Table 2.

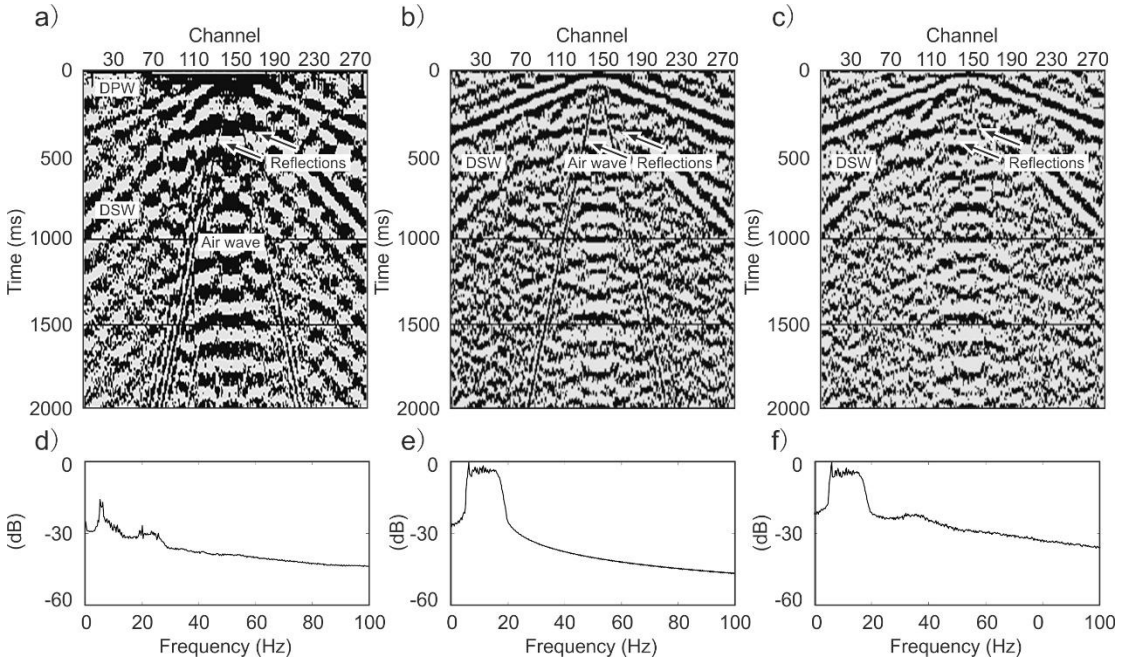

Figure 4: Noise attenuation processing steps from No. 142 source gather. (a) Raw retrieved source gather, DPW and DSW represent the direct P-wave with a velocity of 3700 m/s and the direct S-wave with a velocity of 1700 m/s; (b) after spectral equalization filter (5-6-18-19 Hz); (c) after median filtering to remove noise, air wave 340 m/s; (d), (e) and (f) are power spectra for (a), (b) and (c), respectively.

6 Synthetic seismogram

The acoustic velocity log from the Nore-1 borehole along with a constant density value, 2.7×10^3 kg/m^3, was used to calculate a seismic impedance log and associated reflection coefficients (Fig. 5a). A synthetic seismogram was then produced by convolving the acoustic reflection coefficient with a 10 Hz Ricker wavelet (Fig. 5b). To compare with the passive seismic results, 11 stacked CDP gathers from near the Nore-1 borehole were extracted from the stacked section (Fig. 5c). As shown in Fig. 5b and Fig. 5c, three reflections correlate well between the synthetic seimogram and the passive seismic image at times of 170 ms, 280 ms and 360 ms, indicating that the passive seismic reflection data are trustworthy and can be used for geological interpretation.

https://doi.org/10.5194/egusphere-2025-1325
Preprint. Discussion started: 1 April 2025

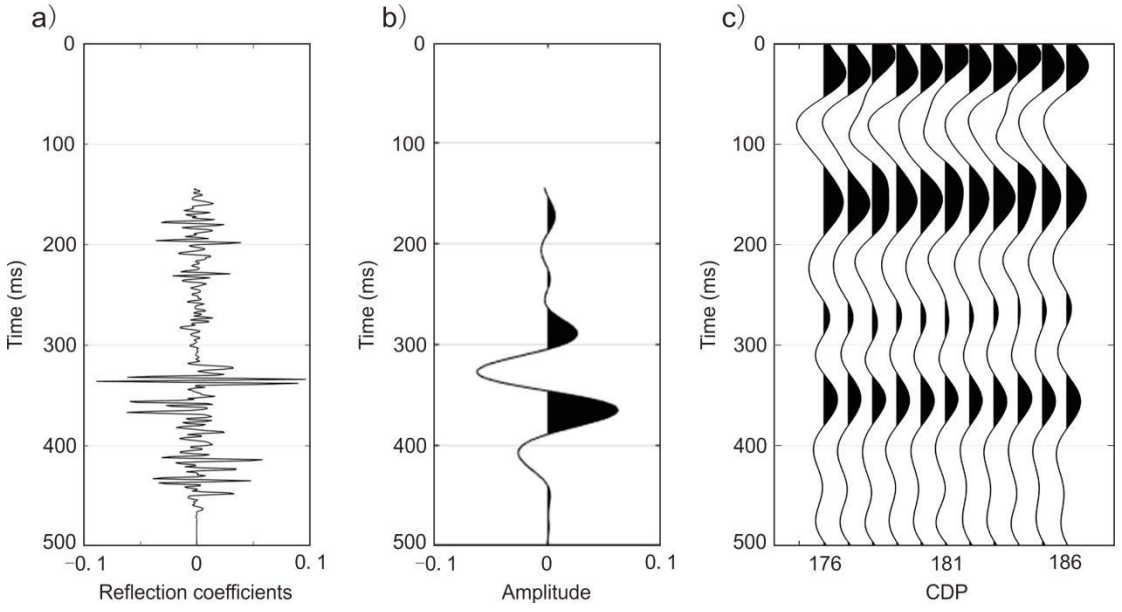

Figure 5: (a) Reflection coefficient curve based on acoustic velocity logging from the Nore-1 borehole and an assumed constant density of 2.7 ×10^3 kg/m^3. (b) Synthetic seismogram produced from convolving (a) with a 10 Hz Ricker wavelet. (c) stacked CDP gathers near borehole Nore-1.

7 Results

7.1 Inverted shear wave velocity model

The extracted surface wave data were inverted for shear wave velocity using the logging data as constraints. The inverted shear wave velocity model shown in Fig. 6a can be interpreted as representing four geological units that can be correlated well with the borehole section (Fig. 6b). From the ground surface to 470 m depth, the velocity increases and varies from 1400 m/s to c. 2600 m/s. A high velocity layer is embedded at the depths of 470 m to 550 m, which corresponds to the Ordovician. Note that the presence of this high velocity layer, and the depth to it, is dependent upon the starting model used, but the results indicate that it is continuous along the profile and the depth to it does not vary. Cambrian rocks are located from 550 m to 780 m. The high velocity under 780 m represents the Precambrian. Moreover, the velocity structure is continuous along the survey line, indicating that there are no potentially large-scale faults in the area. The reliable geological interpretation suggests that passive surface wave inversion results can be used to map the geological strata in the area. Although not proved here, they also have the potential to map regional faults.

https://doi.org/10.5194/egusphere-2025-1325
Preprint. Discussion started: 1 April 2025

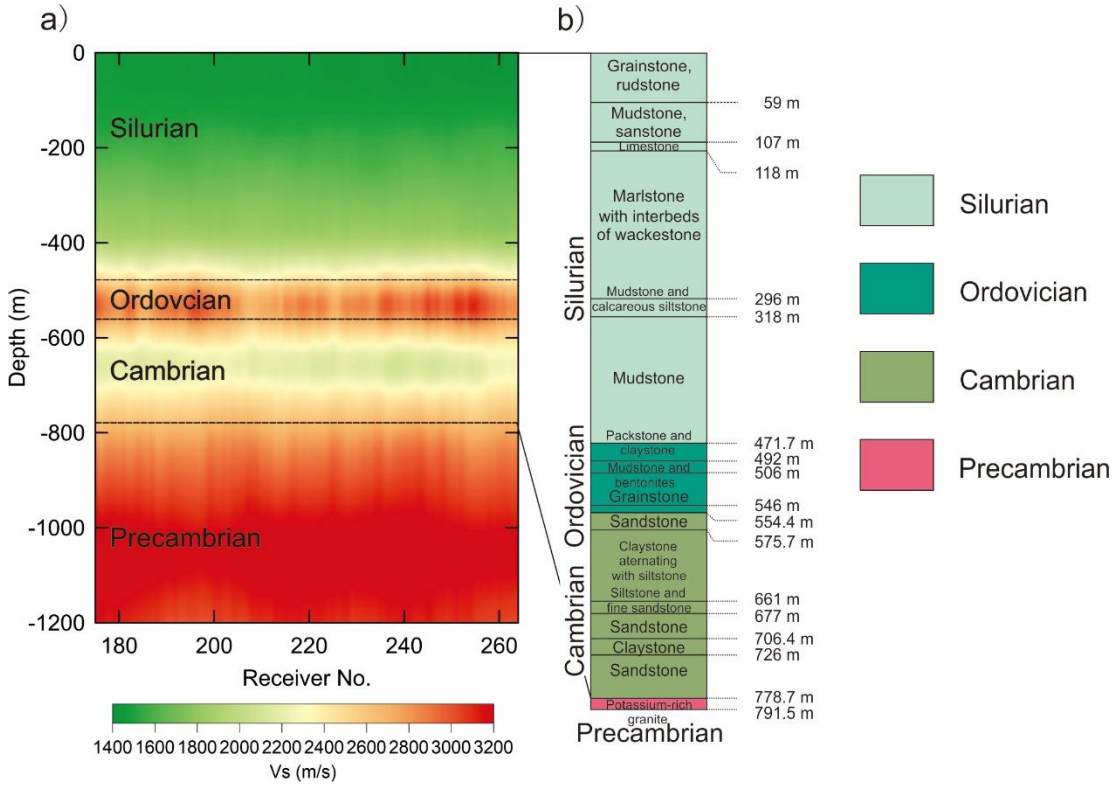

Figure 6: (a) Inverted shear wave velocity from passive surface waves. (b) Nore-1 borehole section.

7.2 Stacked seismic reflection section

Passive source gathers containing body waves (Fig. 4) were processed to test if the passive body wave image can resolve subsurface geological structure. Acoustic logging analyses from Nore-1 at depths of 170 m to 800 m indicated three seismic reflections at travel times of c. 150 ms, 280 ms and 360 ms (labeled as R1, R2 and R3 in Fig. 5) can also be mapped in the stacked section. The uppermost two reflections (R1 and R2) are produced by marlstone with interbeds of wackestone and mudstone from the Silurian, as shown in Fig. 7. The reflection labeled as R3 likely originates from the top of the Ordovician, consistent with logging data and active data (Fig. 8). In addition to the R1, R2 and R3 reflections, another two reflecting horizons are recognized at times of c. 500 ms and 700 ms, labeled as R4 and R5 in Fig. 7. R4 may represent the base of the Cambrian that was interpreted in the active data as the point where the seismic response in the stacked section becomes generally transparent (Juhlin et al., 2025). No borehole or other data are available to validate where R5 originates from, it may originate within the Precambrian or represent a multiple from the top of the Ordovician. As for the inverted shear wave velocity model (Fig. 6a), all reflection horizons shown in Fig. 7 are nearly flat with no obvious disturbances, indicating no large-scale faults are present.

https://doi.org/10.5194/egusphere-2025-1325
Preprint. Discussion started: 1 April 2025

220

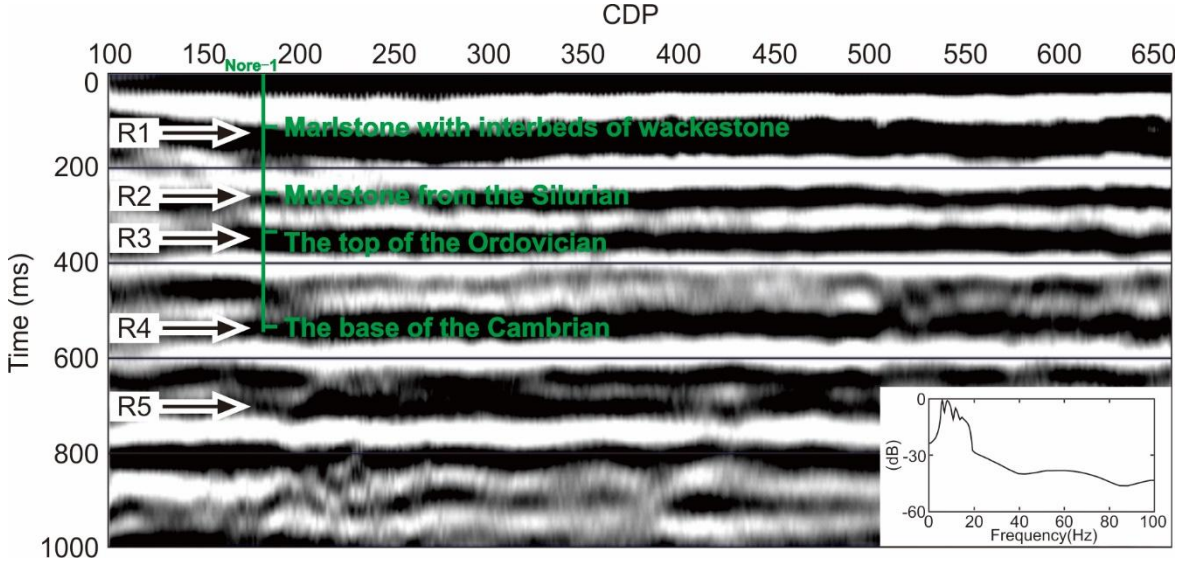

Figure 7: Passive seismic reflection section overlaid with its power spectrum. R1 and R2 represent reflections from the interior of Silurian, R3 represents a reflection from the top of the Ordovician, R4 represents a reflection from the base of the Cambrian, and R5 represents a possible reflection from within the Precambrian or a multiple from the top of the Ordovician.

225

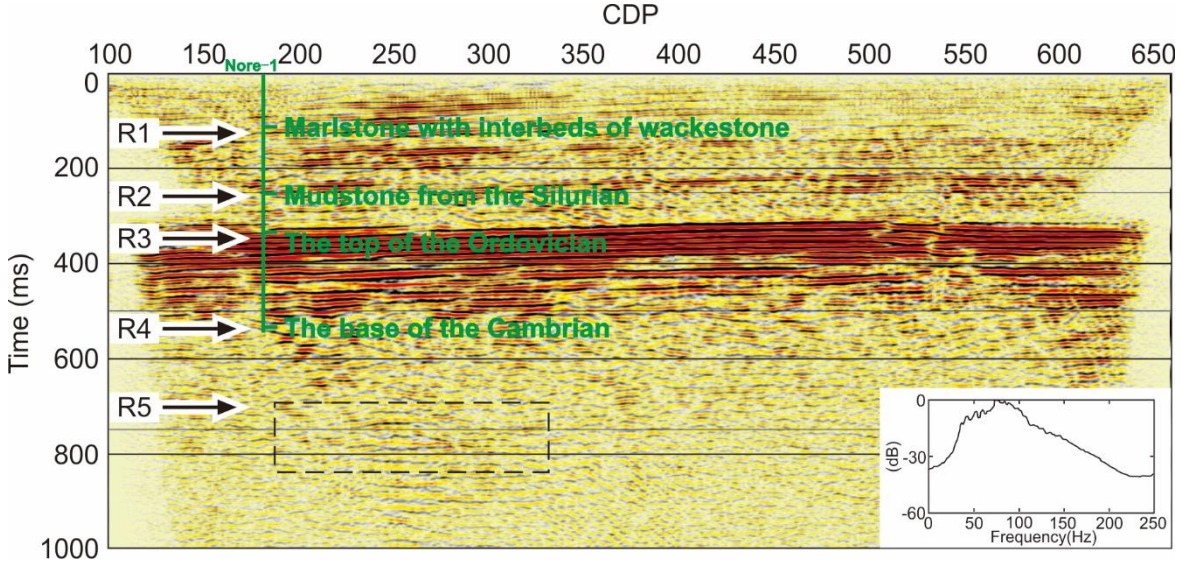

Figure 8: Active seismic reflection stacked section overlaid with its power spectrum (after Juhlin et al., 2025). The dashed box indicates reflected energy that can potentially be correlated with the R5 reflection in the passive stack in Figure 7.

https://doi.org/10.5194/egusphere-2025-1325
Preprint. Discussion started: 1 April 2025

8 Discussion

8.1 Analysis of frequency and direction of ambient noise

To better understand the time-variant nature of the ambient noise sources, 14 one-hour power spectral density panels (Fig. 9) were calculated for every two stations from receiver No. 79 to No. 358 from 17:00 on 12 November, 2023 to 07:00 on 13 November, 2023 (UTC+1). All plots show good consistency except the last one at 06:00-07:00, indicating the frequency components of the noise sources were stable during data acquisition. Ambient noise data were observed at frequencies of 0.5 - 20 Hz in each panel. Four peaks at the frequencies of 1 Hz, 5 Hz, 12 Hz and 16 Hz originate from ocean waves and human activities. These frequencies all contribute to retrieving the virtual source gathers. Particularly, body waves and surface waves can be separated from each other at a frequency of 7 Hz. Surface waves dominate at the frequencies of 0.5 - 7 Hz, whereas body waves dominate at 7 - 20 Hz.

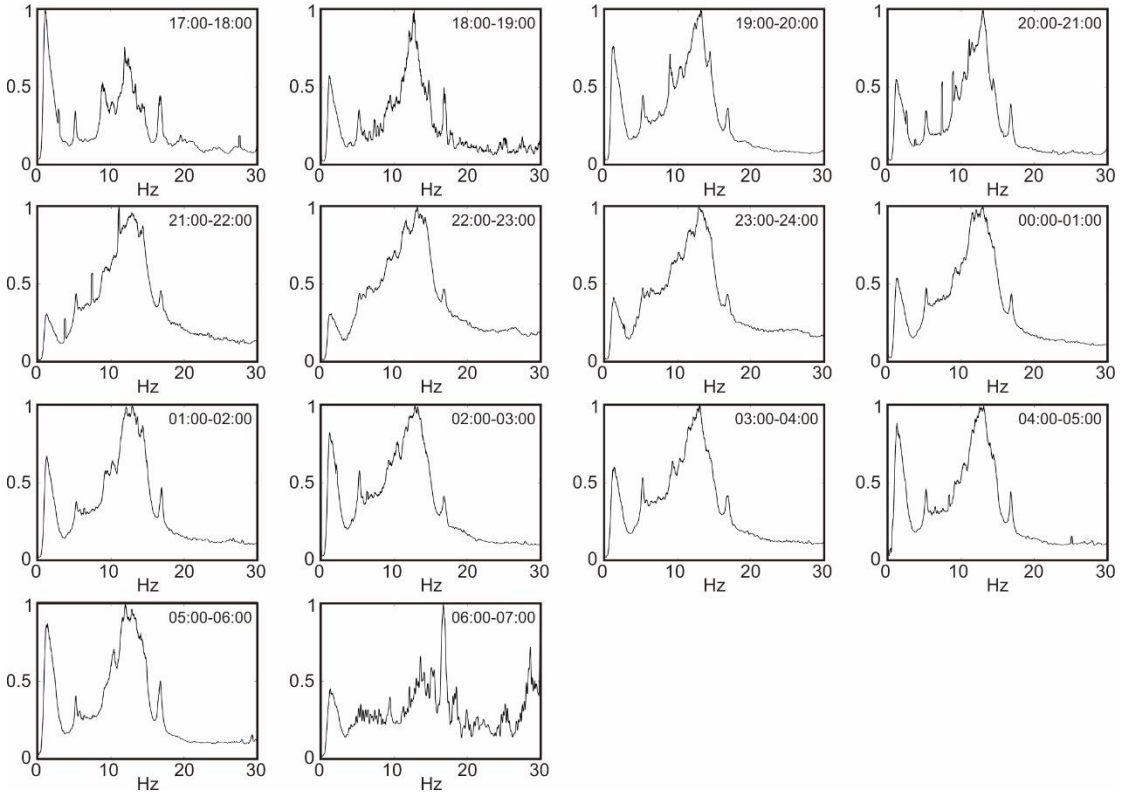

Figure 9: Amplitude spectra normalization of one-hour ambient noise recordings continuously from 17:00 on 12 November, 2023 to 07:00 on 13 November, 2023 (UTC+1).

After the power spectrum density analysis, we evaluate the spatial distributions of the ambient noise sources at the experimental site. A beam forming analysis (Gouédard et al., 2008; Cheraghi et al., 2015) of receiver stations No. 6, No. 49 and No. 185, forming a triangle, was performed with 14-hours of continuous passive data. Fig. 10a and Fig. 10b represent

https://doi.org/10.5194/egusphere-2025-1325
Preprint. Discussion started: 1 April 2025

the maximum values of the beam forming analysis in the frequency ranges of 0.5-7 Hz and 7-20 Hz, respectively. The recorded wavefield of surface waves with a velocity less than 4000 m/s came from the NNW and the azimuth of the ambient noise sources are consistent with the seismic survey line (green lines). The ambient noise sources for the body waves are located in different directions at a velocity higher than 3000 m/s, originating from human activities around the island of Gotland, such as in mainland Sweden, Finland, Estonia, Poland, Germany, Denmark, Norway, etc (Fig. 1a).

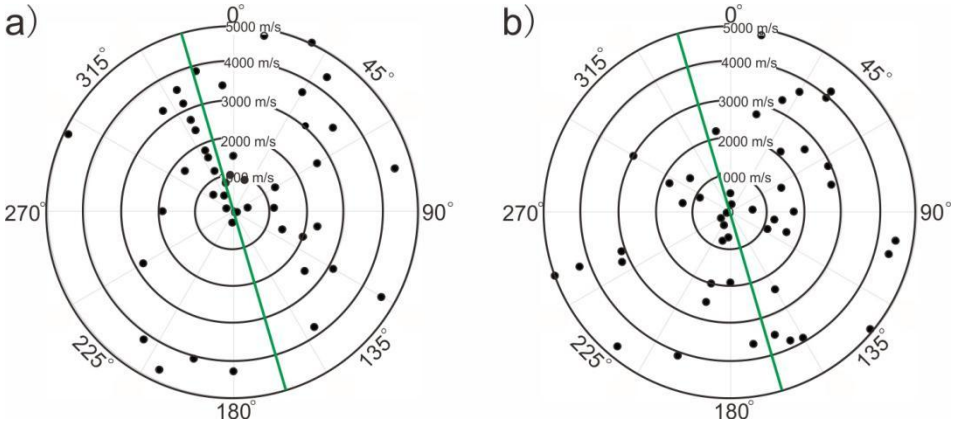

Figure 10: Directional beam forming analysis of ambient sources with different frequency components. (a) The maximum values of normalized strength of source energy at the frequencies of 0.5-7 Hz. (b) The maximum values of normalized strength of source energy at the frequencies of 7 - 20 Hz. The green lines shown in Fig. 10a and Fig. 10b show the azimuth of seismic profile.

8.2 Comparisons of active and passive seismic reflection imaging

The stacked image from the high-resolution active seismic shown in Fig. 8 (Juhlin et al., 2025) indicates that a particularly strong reflection at about 350 ms likely originates from the top of the Ordovician. In addition, Cambrian sandstones below are also reflective, as well as shallow sandstone layers in the upper 150 ms. Reflections labeled R1, R2 and R3 in the active data are consistent with the passive seismic stacked section (Fig. 7). As mentioned previously, R4 may represent a reflection from the top of the crystalline basement. No clear top of basement reflection is observed in the active data, but this may be due to the higher frequency nature of these data. The lower frequencies in the passive data may be more sensitive to the velocity structure near the top of the crystalline basement. There is no clear reflection in the active seismic data that corresponds to the R5 reflection in the passive data. Some indications of reflected energy, interpreted to lie below the crystalline basement can be observed in the active data within the dashed rectangle in Fig. 8. However, it should be noted that the timing of this reflected energy is consistent with a multiple from the top of the Ordovician. The general consistency of the passive seismic data with the active data down to the top of the crystalline basement implies that passive methods can be used to reliably map some of the structural features on Gotland. However, the active data provide a higher resolution image and more geological detail. The power spectra of the passive and active reflection data shown in Fig. 7 and Fig. 8 indicate the dominant frequency ranges for the passive data are 5-20 Hz, while the active data have a 30-200 Hz range.

https://doi.org/10.5194/egusphere-2025-1325
Preprint. Discussion started: 1 April 2025

Consequently, we cannot expect that the passive seismic reflection method will provide the same resolution as the active seismic reflection, but the methodology can be used to map the general structure of the Paleozoic rocks at a low cost.

8.3 Relevance of results for CO_2 storage and seismic imaging

Both the passive surface wave and body wave results provide high-quality images for investigating the subsurface geological structure at the Sudret site. Processing of the passive data allowed us to obtain images of the subsurface down to the Precambrian basement in the vicinity of the Nore-1 borehole that had been core-drilled earlier down to about 800 m. Compared with the active data (Juhlin et al., 2025), these images show major features that can be mapped over a wide area at low cost using passive methods. However, the Sudret site may not represent a typical site for passive seismic imaging given that it is located at the southern tip of an island. This allows noise from nearly all directions to be recorded, which is especially important for body wave imaging. Furthermore, the ambient noise from local sources was very low at the location, allowing far-field noise to be recorded without interference. A next step would be to set up synthetic models to test how much CO_2 is required in the bedrock in order for it to be detectable by the passive methods presented in this paper. The surface waves would be more sensitive to pressure changes in the reservoir, whereas the body waves would be more sensitive to the amount of free CO_2 in the reservoir. It remains to be seen if these passive methods can be used for monitoring CO_2 storage sites in an effective manner.

9 Conclusions

We retrieved virtual shot gathers with body waves and surface waves after applying signal separation through cross coherence and cross correlation calculations. For the body waves, conventional seismic data processing was conducted to obtain a stacked section consistent with active data and a synthetic seismogram generated from an acoustic sonic log. For the surface waves, we determined the dispersion curve in the frequency range 0.8 to 5.5 Hz and inverted these curves to obtain a velocity model that correlates with borehole data from the surface down to c. 800 m. Both the body waves and surface waves provide high-quality images of the top of the Ordovician formation and have a good consistency with the borehole section. These results show that passive data can be used for mapping some general features in the subsurface of Gotland. In particular, the top of the Ordovician and the top of the Precambrian can be mapped. Compared with active seismic exploration, passive seismic is friendly to the environment and cost effective. In some cases, it may have the potential to replace active seismic imaging for initial subsurface surveying of the sedimentary layers on Gotland, and perhaps elsewhere. The method remains to be tested for monitoring CO_2 storage sites.

Data availability

Requests for the seismic data should be directed to SGU (www.sgu.se)

https://doi.org/10.5194/egusphere-2025-1325
Preprint. Discussion started: 1 April 2025

Author contribution

CJ and PH conceptualized and designed this study. ZW and CJ were involved in the data acquisition and responsible for the data processing. ME and DS provided borehole data. ZW and CJ led the geological interpretation. ZW wrote the initial draft and CJ reviewed it. All authors participated in the results discussion and approved the submission of this paper.

Competing interests

The authors acknowledge that there are no conflicts of interest.

Acknowledgments

This research was funded by the Geological Survey of Sweden, the Deep Earth Probe and Mineral Resources Exploration - National Science and Technology Major Project (2024ZD1002201) and the China Geological Survey Project (DD20221819). We acknowledge Dr. Wilczynski Zbigniew from Uppsala University, Dr. Bojan Brodic from University of the Witwatersrand, South Africa and Johan Söderman and Per Wahlquist from the Geological Survey of Sweden who contributed to the data acquisition. Globe Claritas™ under the academic license from Petrosys Ltd. and Seismic Unix was used for the data processing.

References

Alcalde, J., Marzán, I., Saura, E., Martí, D., Ayarza, P., Juhlin, C., Pérez-Estaún, A., and Carbonell, R.: 3D geological characterization of the Hontomín CO_2 storage site, Spain: Multidisciplinary approach from seismic, well-log and regional data, Tectonophysics, 627, 6–25, doi:10.1016/j.tecto.2014.04.025, 2014.

Anthonsen, K. L., Aagaard, P., Bergmo, P. E. S., Erlström, M., Fareide, J. I., Gislason, S. R., et al.: CO_2 storage potential in the Nordic region, Energy Procedia, 37, 5080–5092, doi:10.1016/j.egypro.2013.06.421, 2013.

Bakulin, A., and Calvert, R.: The virtual source method: Theory and case study, Geophysics, 71(4), SI139–SI150, doi:10.1190/1.2216190, 2006.

Boullenger, B., Verdel, A., Paap, B., Thorbecke, J., and Draganov, D.: Studying CO_2 storage with ambient-noise seismic interferometry: A combined numerical feasibility study and field-data example for Ketzin, Germany, Geophysics, 80(2), Q1–Q13, doi:10.1190/geo2014-0181.1, 2015.

Campillo, M., and Paul, A.: Long-range correlations in the diffuse seismic coda, Science, 299(5606), 547–549, doi:10.1126/science.1078551, 2003.

Cao, H., and Askari, R.: Comparison of seismic interferometry techniques for the retrieval of seismic body waves in CO_2 sequestration monitoring, Journal of Geophysics and Engineering, 16(6), 1094–1115, doi:10.1093/jge/gxz079, 2019.

https://doi.org/10.5194/egusphere-2025-1325
Preprint. Discussion started: 1 April 2025

Cheraghi, S., Craven, J. A., and Bellefleur, G.: Feasibility of virtual source reflection seismology using interferometry for mineral exploration: A test study in the Lalor Lake volcanogenic massive sulphide mining area, Manitoba, Canada, Geophysical Prospecting, 63(4), 833–848, doi:10.1111/1365-2478.12244, 2015.

Cheraghi, S., White, D. J., Draganov, D., Bellefleur, G., Craven, J. A., and Roberts, B.: Passive seismic reflection interferometry: A case study from the Aquistore CO_2 storage site, Saskatchewan, Canada, Geophysics, 82(4), B79–B93, doi:10.1190/geo2016-0370.1, 2017.

Claerbout, J. F.: Synthesis of a layered medium from its acoustic transmission response, Geophysics, 33(2), 264–269, doi:10.1190/1.1439927, 1968.

Oren, C., and Nowack, R. L.: Seismic body-wave interferometry using noise autocorrelations for crustal structure, Geophysical Journal International, 208(1), 321–332, doi:10.1093/gji/ggw394, 2017.

Cole, S. P.: Passive seismic and drill-bit experiments using 2-D arrays, California: Stanford University, 1995.

De Ridder, S., and Biondi, B.: Continuous passive seismic monitoring of CCS projects by correlating seismic noise – A feasibility study, 74th Annual International Conference and Exhibition, EAGE, Extended Abstracts, P253, 2012.

Draganov, D., Campman, X., Thorbecke, J., Verdel, A., and Wapenaar, K.: Reflection images from ambient seismic noise, Geophysics, 74(5), A63–A67, doi:10.1190/1.3193529, 2009.

Erlström, M., Sopher, D.: Geophysical well log-motifs, lithology, stratigraphical aspects and correlation of the Ordovician succession in the Swedish part of the Baltic Basin. International Journal of Earth Sciences, 108, 1387-1407. doi:10.1007/s00531-019-01712-y, 2019.

Erlström, M., Rosberg, J.E., Dahlqvist, P., Hjerne, C-E., Lorenz, H.: Scientific core drilling of the Lower Palaeozoic succession in the Swedish sector of the Baltic Sea - investigation of the CO_2 storage potential, European Geosciences Union General Assembly 2024, doi:10.5194/egusphere-egu24-5974, 2024.

Gassenmeier, M., Sens-Schönfelder, C., Delatre, M., and Korn, M.: Monitoring of environmental influences on seismic velocity at the geological storage site for CO_2 in Ketzin (Germany) with ambient seismic noise, Geophysical Journal International, 200(1), 524–533, doi:0.1093/gji/ggu413, 2015.

Gouédard, P., Stehly, L., Brenguier, F., Campillo, M., Colin de Verdière, Y., Larose, E., Margerin, L., Roux, P., Sánchez-Sesma, F. J., Shapiro, N. M., and Weaver, R. L.: Cross-correlation of random fields: Mathematical approach and applications, Geophysical Prospecting, 56(3), 375–393, doi:0.1111/j.1365-2478.2007.00684.x, 2008.

Harris, K., White, D., and Samson, C.: Imaging the Aquistore reservoir after 36 kilotonnes of CO_2 injection using distributed acoustic sensing, Geophysics, 82(6), M81–M96, doi:0.1190/geo2017-0174.1, 2017.

Hassing, S. H. W., Draganov, D., Janssen, M., Barnhoorn, A., Wolf, K.-H. A. A., van den Berg, J., Friebel, M., van Otten, G., Poletto, F., Bellezza, C., Barison, E., Brynjarsson, B., Hjörleifsdóttir, V., Obermann, A., Sánchez-Pastor, P., and Durucan, S.: Imaging CO_2 reinjection into basalts at the Carbfix2 reinjection reservoir (Hellisheiði, Iceland) with body-wave seismic interferometry, Geophysical Prospecting, 72(5), 1919–1933, doi:0.1111/1365-2478.13472, 2024.

https://doi.org/10.5194/egusphere-2025-1325
Preprint. Discussion started: 1 April 2025

Huang, F., Bergmann, P., Juhlin, C., Ivandic, M., Lüth, S., Ivanova, A., Kempka, T., Henninges, J., Sopher, D., and Zhang, F.: The first post-injection seismic monitor survey at the Ketzin pilot CO_2 storage site: Results from time-lapse analysis, Geophysical Prospecting, 66(1), 62–84, doi:0.1111/1365-2478.12497, 2016.

Ikeda, T., Tsuji, T., Takanashi, M., Kurosawa, I., Nakatsukasa, M., Kato, A., Worth, K., White, D., and Roberts, B.: Temporal variation of the shallow subsurface at the Aquistore CO_2 storage site associated with environmental influences using a continuous and controlled seismic source, Journal of Geophysical Research: Solid Earth, 122(4), 2859–2872, doi:0.1002/2016JB013691, 2017.

Ivandic, M., Bergmann, P., Kummerow, J., Huang, F., Juhlin, C., and Lüth, S.: Monitoring CO_2 saturation using time-lapse amplitude versus offset analysis of 3D seismic data from the Ketzin CO_2 storage pilot site, Germany, Geophysical Prospecting, 66(8), 1568–1585, doi:0.1111/1365-2478.12666, 2018.

Juhlin, C., Erlström, M., Hedin, P., Brodic, B. and Sopher, D.: Reflection seismic investigations on south Gotland, Sweden, to evaluate CO_2 storage strategies, egusphere-2025-938.

Juhlin, C., Giese, R., Zinck-Jørgensen, K., Cosma, C., Kazemeini, H., Juhojuntti, N., Lüth, S., Norden, B., and Förster, A.: 3D baseline seismics at Ketzin, Germany: The CO2SINK project, Geophysics, 72(5), B121–B132, doi:0.1190/1.2754667, 2007.

Lüth, S., Bergmann, P., Huang, F., Ivandic, M., Ivanova, A., Juhlin, C., and Kempka, T.: 4D seismic monitoring of CO_2 storage during injection and post-closure at the Ketzin pilot site, Energy Procedia, 114, 5761–5767, doi:0.1016/j.egypro.2017.03.1714, 2017.

Meles, G. A., Löer, K., Ravasi, M., Curtis, A., and da Costa Filho, C. A.: Internal multiple prediction and removal using Marchenko autofocusing and seismic interferometry, Geophysics, 80(2), A7–A11, doi:0.1190/geo2014-0408.1, 2015.

Nakata, N., Snieder, R., Tsuji, T., Larner, K., and Matsuoka, T.: Shear wave imaging from traffic noise using seismic interferometry by cross-coherence, Geophysics, 76(6), SA97–SA106, doi:0.1190/geo2010-0188.1, 2011.

Nakata, N., Chang, J. P., Lawrence, J. F., and Boué, P.: Body wave extraction and tomography at Long Beach, California, with ambient-noise interferometry, Journal of Geophysical Research: Solid Earth, 120(2), 1159–1173, doi:0.1002/2015JB011870, 2015.

Niemi, A., Bear, J., and Bensabat, J.: Geological storage of CO_2 in deep saline formations, Geological Storage of CO_2 in Deep Saline Formations, 2017.

Olivier, G., Brenguier, F., Campillo, M., Lynch, R., and Roux, P.: Body-wave reconstruction from ambient seismic noise correlations in an underground mine, Geophysics, 80(5), KS11–KS25, doi:0.1190/geo2014-0299.1, 2015.

Papadopoulou, M., Zappalá, S., Malehmir, A., Gregersen, U., Hjelm, L., Nielsen, L., and Haspang, M. P.: Innovative land seismic investigations for CO_2 geologic storage in Denmark, Geophysics, 88(4), B251–B266, doi:0.1190/geo2022-0693.1, 2023.

https://doi.org/10.5194/egusphere-2025-1325
Preprint. Discussion started: 1 April 2025

Papadopoulou, M., Zappalá, S., Malehmir, A., Kucinskaite, K., Westgate, M., Gregersen, U., Funck, T., Smit, F., and Vosgerau, H.: Advancements in seismic imaging for geological carbon storage: Study of the Havnsø structure, Denmark, International Journal of Greenhouse Gas Control, 137, doi:0.1016/j.ijggc.2024.104204, 2024.

Pevzner, R., Caspari, E., Gurevich, B., Dance, T., and Cinar, Y.: Feasibility of CO_2 plume detection using 4D seismic: CO2CRC Otway project case study – Part 2: Detectability analysis, Geophysics, 80(2), B105–B114, doi:0.1190/geo2014-0460.1, 2015.

Prieto, G. A., Lawrence, J. F., and Beroza, G. C.: Anelastic Earth structure from the coherency of the ambient seismic field, Journal of Geophysical Research: Solid Earth, 114(B7), doi:0.1029/2008JB006067, 2009.

Riahi, N., Bokelmann, G., Sala, P., and Saenger, E. H.: Time-lapse analysis of ambient surface wave anisotropy: A three-component array study above an underground gas storage, Journal of Geophysical Research: Solid Earth, 118(10), 5339–5351, doi:0.1002/jgrb.50375, 2013.

Rickett, J., and Claerbout, J.: Acoustic daylight imaging via spectral factorization: Helioseismology and reservoir monitoring, The Leading Edge, 18(8), 957–960, doi:0.1190/1.1438420, 1999.

Roach, L. A. N., White, D. J., and Roberts, B.: Assessment of 4D seismic repeatability and CO_2 detection limits using a sparse permanent land array at the Aquistore CO2 storage site, Geophysics, 80(5), WA1–WA13, doi:0.1190/geo2014-0201.1, 2015.

Schuster, G. T.: Theory of daylight/interferometric imaging – Tutorial, 2001.

Shapiro, N. M., Campillo, M., Stehly, L., and Ritzwoller, M. H.: High-resolution surface-wave tomography from ambient seismic noise, Science, 307(5715), 1615–1618, doi:0.1126/science.1108339, 2005.

Shogenova, A., Nordback, N., Sopher, D., Shogenov, K., Niemi, A., Juhlin, C., Sliaupa, S., Ivandic, M., Wojcicki, A., Ivask, J., Klimkowski, L., and Nagy, S.: Carbon neutral Baltic Sea region by 2050: Myth or reality?, SSRN Electronic Journal, doi:0.2139/ssrn.3817722, 2021.

Snieder, R.: Extracting the Green's function from the correlation of coda waves: A derivation based on stationary phase, Physical Review E, 69(4), doi:0.1103/PhysRevE.69.046610, 2004.

Sopher, D., Juhlin, C., and Erlström, M.: A probabilistic assessment of the effective CO_2 storage capacity within the Swedish sector of the Baltic Basin, International Journal of Greenhouse Gas Control, 30, 148–170, doi:0.1016/j.ijggc.2014.09.009, 2014.

Wang, Y., and Lawton, D. C.: Time-lapse attenuation variations using distributed acoustic sensing vertical seismic profile data during CO_2 injection at Cami Field Research Station, Alberta, Canada, Geophysics, 89(3), N31–N44, doi:0.1190/geo2022-0731.1, 2024.

Wang, Z., Juhlin, C., Hedin, P., Erlström, M., and Sopher, D.: Passive seismic imaging for CO_2 geological storage in the Sudret area of Gotland, Sweden, EGU General Assembly Conference Abstracts, doi:0.5194/egusphere-egu24-8975, 2024.

https://doi.org/10.5194/egusphere-2025-1325
Preprint. Discussion started: 1 April 2025

Wapenaar, K., Thorbecke, J., and Draganov, D.: Relations between reflection and transmission responses of three-dimensional inhomogeneous media, Geophysical Journal International, 156(1), 179–194, doi:0.1111/j.1365-246X.2003.02152.x, 2004.

Wapenaar, K., and Fokkema, J.: Green's function representations for seismic interferometry, Geophysics, 71(4), SI33–SI46, doi:0.1190/1.2213955, 2006.

White, D. J., Roach, L. A. N., and Roberts, B.: Time-lapse seismic performance of a sparse permanent array: experience from the Aquistore CO_2 storage site, Geophysics, 80, WA35–WA48, doi:0.1190/geo2014-0239.1, 2015.

White, D., Bellefleur, G., Dodds, K., and Movahedzadeh, Z.: Toward improved distributed acoustic sensing sensitivity for surface-based reflection seismics: Configuration tests at the Aquistore CO_2 storage site, Geophysics, 87(3), P1–P14, doi:0.1190/geo2021-0120.1, 2022.

Xu, Z., Juhlin, C., Gudmundsson, O., Zhang, F., Yang, C., Kashubin, A., and Lüth, S.: Reconstruction of subsurface structure from ambient seismic noise: an example from Ketzin, Germany, Geophysical Journal International, 189, 1085–1102, doi:0.1111/j.1365-246X.2012.05411.x, 2012.

Zappalà, S., Malehmir, A., Papadopoulou, M., Gregersen, U., Funck, Clausen, O. R., and Nørmark, E.: Combined onshore and offshore wide-scale seismic data acquisition and imaging for carbon capture and storage exploration in Havnsø, Denmark, Geophysics, 89, B257–B272, doi:0.1190/geo2023-0503.1, 2024.

Zhang, F., Juhlin, C., Niemi, A., Huang, F., and Bensabat, J.: A feasibility and efficiency study of seismic waveform inversion for time-lapse monitoring of onshore CO_2 geological storage sites using reflection seismic acquisition geometries, International Journal of Greenhouse Gas Control, 48, 134–141, doi:10.1016/j.ijggc.2015.11.015, 2016.

Zhao, D., Wang, G., Wang, S., and Sun, R.: The application of genetic algorithm to Rayleigh wave inversion (in Chinese), Geophysical & Geochemical Exploration, 19, 178–185, 1995.